A comparison of forecasting techniques applied to Droughts in North America

by

Erick Armando Díaz Cadena

An Extended Essay Submitted in Partial Fulfillment
of the Requirements for the Degree of

MASTER OF ARTS

in the Department of Economics
University of Victoria

Dr. Felix Pretis, Supervisor (Department of Economics)

Dr. Graham M. Voss, Member (Department of Economics)

Abstract

Droughts have a substantial socio-economic impact, and their severity and duration are only being exacerbated by climate change. Understanding the dynamics of droughts is important for enabling societies to adapt and create policies to mitigate their effects. Droughts are measured using indices; one of those is the Standardized Precipitation Evapotranspiration Index (SPEI). In this essay, I train and analyze the performance of 4 different forecasting methodologies: Seasonal ARIMA, Machine Learning techniques such as Random Forests and Artificial Neural Networks, and Hybrid models using Wavelet Transformation + ARIMA. I compare the forecast performance using RMSE and MAE indicators, as well as the Diebold-Mariano Test. I work with a gridded global database of SPEI, which allows us to train models and produce forecasts at a pixel level. Given the geographic focus on the North America Region (Canada, the United States, and Mexico), I conclude that Seasonal ARIMA models achieve the lowest RMSE overall, but their forecasting power is geographically dependent. Other models perform better depending on geography. In very few locations, the lowest-RMSE model shows a statistically significant difference according to the Diebold-Mariano Test.

Contents

1 Introduction and Motivation

Droughts have a substantial socio-economic impact, and the magnitude, severity, and duration are only being exacerbated by global warming (Gebrechorkos et al., 2025). According to the IPCC AR6 Synthesis Report—Section 3, "Long-Term Climate and Development Futures"— (IPCC, 2023), global warming will lead to long-term changes in key climatological variables such as precipitation and soil moisture, as well as a more widespread propensity to extremes that will reflect into more and more intense droughts.

Studying this phenomenon from an economic perspective is essential given its wide range of potential consequences. Severe drought generates serious effects, including lower agricultural yields (Gouveia, Trigo, & DaCamara, 2009) or reduced water supply to populated areas (Gober, Sampson, Quay, White, & Chow, 2016), disruptions to hydroelectric power (Azouaoui & Assani, 2018), or even disruptions to the global supply chain, e.g., the Panama Canal (Aguilar & Naranjo, 2022). Droughts require substantial investments in water management infrastructure and other adaptation measures. According to the United Nations Convention to Combat Desertification, addressing drought impacts may require up to US$210 billion in planned investments worldwide (Thomas et al., 2024). To forecast drought conditions, understanding their dynamics is fundamental to creating policies and planning ahead.

In this Essay, I apply different econometric models to forecast droughts. I implement Seasonal ARIMA models, hybrid models combining wavelet transformation with Seasonal ARIMA, and machine learning models, including Random Forests and Artificial Neural Networks. I compare the forecasting power of these methods using the Root Mean Square Error (RMSE) and the Mean Absolute Error (MAE), and perform a Diebold-Mariano test.

This Essay focuses on the North American region (Canada, the United States, and Mexico). North America offers a wide range of climates and environments to compare the performance of each model. A main contribution to the literature is the use of a gridded dataset

of North America to forecast drought conditions with the regional climatological dynamics.

Dracup, Lee, and Paulson (1980) and Wilhite and Glantz (1985) agreed that there is a lack of a single definition of drought. They also coincide in the categories of drought: meteorological, agricultural, hydrological, and socio-economic. They define meteorological droughts as the balance between precipitation and potential evapotranspiration. Agricultural droughts are related to precipitation and the soil moisture required by crops; hydrological droughts are related to reduced water levels in rivers or reservoirs; and socio-economic droughts are related to water shortages that affect the availability of resources to the population.

Other efforts to define the drought come along with methodologies to measure it. To measure drought, the literature has focused on developing drought indices. The Handbook of Drought Indicators and Indices from the World Meteorological Organization provides a list of more than 50 indicators and indices (World Meteorological Organization & Global Water Partnership, 2016). One of the first attempts is the Palmer Drought Severity Index (PDSI), introduced by Palmer (1965). The PDSI incorporates a water balance model that accounts for both supply (precipitation) and demand (soil moisture and evapotranspiration). The disadvantages of this methodology are the need for calibration to effectively measure droughts in each region and the inability to measure droughts across different time scales.

These disadvantages were addressed by the introduction of the Standardized Precipitation Index (SPI) by McKee, Doesken, and Kleist (1993). For the SPI, the definition of drought is based on the precipitation deficit: the difference between the actual precipitation (P_t) and the long-term levels of precipitation ($\bar{P}$). The authors recommend a 30-year period for a long-run mean. Precipitation and long-run precipitation can be calculated on different time scales: 3, 6, 12, 24, or 48 months.

The contribution of SPI to the drought index literature was the standardisation process. An intuitive way to think of a standardization process is to divide the precipitation deficit by the standard deviation of the same long-term period (S_P). However, the author clarifies that

precipitation data is not normally distributed, invalidating this approach. To address this problem, the proposed approach is to fit the precipitation data into a Gamma Distribution. Now, with an established relationship between observed precipitation and the probability of observing it, the probability is associated with a Normal Distribution using an estimate of the inverse standard normal cumulative distribution function. After the standardisation process, the SPI Index is essentially a Z-score. The SPI simplified the data requirements compared to PDSI and enabled the possibility of generating a multiscalar index. The disadvantage was the simplified definition of drought, which does not account for evapotranspiration or other variables related to water demand.

The Standardized Precipitation Evapotranspiration Index (SPEI) was introduced by Vicente Serrano, Beguería, and López-Moreno (2010). The SPEI is developed from the SPI; it is also a multiscalar index and follows a standardisation process. The main difference is that, for the SPEI, the definition of drought includes not only precipitation but also Potential Evapotranspiration (PET). Effectively solving the disadvantages of the SPI with minimal increase in data and processing.

The PET definition used is from Thornthwaite (1948), who defined PET as the amount of water that could be evaporated or transpired if available. This includes both sides of the water balance equation: the supply of water to the soil and the demand for water from the system.

The calculation of the SPEI starts with the balance in the water equation defined as D_t being equal to the difference between the precipitation P and the Potential Evapotranspiration PET for a given month t. The Equation (1) summarise it:

$$D_t = P_t - PET_t \tag{1}$$

The PET calculation methodology used by the authors follows the methodology described by Thornthwaite (1948). In the methodology, PET is a function of temperature, a heat index,

and the hours of sunlight in a given month, all of which vary by geographic location. The PET calculation is comprehensive, accounts for several physical variables, and is designed to compare different geographies and climates.

The values for D_t are aggregated to the desired time scale. For the standardization process, the process followed is to fit the value of the aggregated D_t into a Log-Logistic Distribution. The authors selected this distribution after testing several others, including the gamma distribution followed in SPI. The log-logistic distribution was chosen because it performed better across different geographies. The final step, as in SPI, is to associate the probability with a Normal Distribution using an estimate of the inverse standard normal cumulative distribution function.

The standardization process produces an indicator that is comparable over time and space, with a mean of 0 and a variance of 1. As an additional benefit, it also relates to a Z-score widely known in statistics.

The SPEI is usually translated into a qualitative drought characteristic. The Table 1 summarizes the different classifications of droughts based on SPEI values. An intuitive approach to extreme events in SPEI is the Z-score definition. Only 5% of the events fall beyond ± 1.96, characterizing the extremes. A deviation of ± 0.5 from the mean of 0 is categorized as a wet event or a drought event.

Table 1: Categorization of drought/wet conditions according to SPEI

Category	**SPEI value range**
Extremely wet	$\text{SPEI} \geq 2.0$
Very wet	$1.5 \leq \text{SPEI} < 2.0$
Moderately wet	$1.0 \leq \text{SPEI} < 1.5$
Mildly wet	$0.5 \leq \text{SPEI} < 1.0$
Normal	$-0.5 \leq \text{SPEI} < 0.5$
Mild drought	$-1.0 \leq \text{SPEI} < -0.5$
Moderate drought	$-1.5 \leq \text{SPEI} < -1.0$
Severe drought	$-2.0 \leq \text{SPEI} < -1.5$
Extreme drought	$\text{SPEI} \leq -2.0$

In this Essay, the forecasted variable is the SPEI Index, specifically, the SPEI-12. The database used is the SPEI Global Database published by the same authors (Beguería, Vicente Serrano, Reig-Gracia, and Latorre Garcés (2024)).

This Essay is structured as follows: in Chapter 2, I provide a literature review focusing on forecasting methods, studies on drought forecasting, and tools for comparing forecasts. Chapter 3 describes the Database used for this study. Chapter 4 covers the Methodology,explaining in detail the process followed. Chapter 5 presents the Results, and Chapter 6 concludes and outlines potential next steps for this topic.

2 Literature Review

2.1 Methods and Applications in Drought Forecasting

Traditional time-series models, particularly ARIMA and Seasonal ARIMA (S-ARIMA), remain among the most widely used techniques in drought forecasting. For example, Achite et al. (2022), Mishra and Desai (2005), and Durdu (2010) employ Seasonal ARIMA models to forecast drought indices.

More recent studies increasingly rely on machine-learning methods. Random forest models have been applied in diverse contexts, including Q. Wang et al. (2022), Hussain et al. (2025), and Dikshit, Pradhan, and Alamri (2020). Artificial Neural Networks (ANN) are applied as well by Morid, Smakhtin, and Bagherzadeh (2007). A common practice in the machine learning literature is to present a wide variety of methods, among them Oyounalsoud, Yilmaz, Abdallah, and Abdeljaber (2024), Yaseen, Ali, Sharafati, Al-Ansari, and Shahid (2021), and Gupta et al. (2024) include Random Forest and ANN, among other methodologies. Another technique in the literature is Wavelet Transformation, which should be used in combination with ARIMA or Machine Learning methods, and is used by Rezaiy and Shabri (2023), Khan, Muhammad, and El-Shafie (2020), and Wu et al. (2021).

More details on the methods and studies are provided in the next sections. The main

methodology followed in this Essay was developed based on these studies.

2.1.1 Seasonal ARIMA Model

ARIMA stands for Autoregressive Integrated Moving Average Model. Formalised by Box, Jenkins, and Reinsel (1994), the ARIMA model is defined as $ARIMA(p, d, q)$ where p is the auto-regressive order defined as the number of lagged values of the series included in the model. The moving average order is represented as q, meaning how many past error terms influence the current observations of the variable. Last, d specifies the degree of differencing required.

A development from the ARIMA also included in Box et al. (1994) is the Seasonal ARIMA (S-ARIMA) models, defined as $ARIMA(p, d, q)(P, D, Q)[s]$. Where P, D, Q are respectively the seasonal autoregressive order, the seasonal differencing order, and the seasonal moving average order. s is the seasonal period, which is commonly 12 if the data is monthly, or 4 if the data is quarterly. The functional form is as follows:

$$\Phi(B^s)\,\phi(B)\,(1-B)^d(1-B^s)^D y_t = \Theta(B^s)\,\theta(B)\,\varepsilon_t, \tag{2}$$

Where: $\phi(B) = 1 - \phi_1 B - \phi_2 B^2 - \cdots - \phi_p B^p$ is the AR order, $\theta(B) = 1 + \theta_1 B + \theta_2 B^2 + \cdots + \theta_q B^q$ is the MA order and $\Phi(B^s) = 1 - \Phi_1 B^s - \Phi_2 B^{2s} - \cdots - \Phi_P B^{Ps}$ is the Seasonal AR Order, $\Theta(B^s) = 1 + \Theta_1 B^s + \Theta_2 B^{2s} - \cdots + \Theta_Q B^{Qs}$ the seasonal MA order.

A common approach in ARIMA models is to use information criteria to select a model that balances fitness and complexity. The indicators used are the Akaike Information Criterion (AIC) (Akaike, 1974) and the Bayesian Information Criterion (BIC) (Schwarz, 1978). By design, these indicators penalise the increase in the likelihood value from a more complex model. The criteria are defined as follows:

$$AIC = -2\ln L + 2k \tag{3}$$

and

$$BIC = -2 \ln L + k \ln n \tag{4}$$

, where k is the number of parameters estimated in the model, and L is the value of the likelihood function. The selected model will be the one with the lowest AIC or BIC, respectively.

One of the papers following S-ARIMA models is Achite et al. (2022), which uses it to forecast Drought Indices such as SPI (Standardised Precipitation Index) and SRI (Standardised Runoff Index). The region they focus on is the Wadi Ouahrane Basin in Algeria, and they have precipitation data from 1972 to 2018 (46 years). The model identification process they follow is to iterate over different model specifications and select one using Information Criteria AIC and BIC. Their procedure selected the models ARIMA(1,0,0)(2,0,1)[12] for SPI-12 and ARIMA(0,1,0)(0,1,1)[12] for SRI-12. For model testing, they use the years 2011-2017. They evaluate and test the model using correlation coefficient R^2, Mean Absolute Error (MAE), and Root Mean Squared Error (RMSE). They conclude that the model produces a reasonable adjusted forecast over 12 months.

Another study is Mishra and Desai (2005), which uses S-ARIMA models to forecast drought. They focus only on SPI and the geographic region of the Kansabati river basin in India. They compute an SPI at different time scales using data from five raingauge stations, spanning from 1965 to 1994 (29 years). To select the model, they use the Information Criteria methodology, AIC, and BIC. The chosen model for SPI-12 was ARIMA(1,0,0)(2,1,0)[12]. They run residual diagnostics, including tests for autocorrelation, conditional heteroskedasticity, and normality. For the testing part, they use data from 1994 to 2001. Their conclusions are that the model provides reasonably good results with up to 2 months of lead time, and the precision decreases over time. Durdu (2010) follows the same methodology, using S-ARIMA models to predict drought in the Büyük Menderes River basin in Turkey. They forecast SPI and used data from 1975 to 2006 (31 years).

It is worth noting that other authors also use an S-ARIMA model, but with a different data-collection approach. Mossad and Alazba (2015) studied a region in Saudi Arabia, characterised by a hyper-arid climate. They use SPEI and use data from 1950 to 1989. They use the same database I use in this study, the SPEI Global Database (Beguería et al. (2024)). Although they do not exploit the gridded characteristics. Another study with particularities with the data is Al Sayah, Abdallah, Khouri, Nedjai, and Darwich (2021). They study drought in Lebanon, which has a Mediterranean climate. They extract data and produce simple drought indices from remote-sensing databases like LANDSAT, which can also be reproduced in other geographies.

2.1.2 Machine Learning models: Random Forest & Artificial Neural Network

Most recent papers on drought forecasting are leaning towards machine learning methods. In this Essay, I focused on Random Forest and Artificial Neural Networks.

Random Forest methodology was introduced by Breiman (2001) and is based on his earlier work on decision trees and bootstrap aggregation Breiman (1996). A decision tree recursively splits the data using explanatory variables to classify and later use this classification to predict a dependent variable. Breiman (1996), demonstrated that predictive accuracy improves when multiple decision trees are built on different bootstrap samples of the original dataset and their predictions are averaged.

In Random Forest, the process is extended by creating n_{trees} decision trees, each trained on its own bootstrap sample of the training data. Then, adding an additional layer of randomness: at every split within a tree, only a random subset of predictors, m_{try}, is considered as candidates for splitting. Each tree produces its own prediction, and these predictions are aggregated (averaged when using continuous data). Growing more trees yields a more stable and accurate forecast. The predicted data will be the average across all trees. The process is also explained in Liaw and Wiener (2007). The parameters, called hyperparameters in the

literature, that need to be chosen by the researcher are n_{trees} and m_{try}. This process is often iterative and is called tuning.

In drought forecasting literature, Q. Wang et al. (2022) uses a random forest to predict the value of SPEI-06. They rely on remote-sensing databases (MODIS and GPM). The geographic area is Inner Mongolia, in China. They do not train the model using lags; they exploit the richness of the databases and use variables such as Precipitation Status Index, Temperature Status Index, Enhanced Vegetation Index, Elevation, and terrain slope. The tuning process decides the optimal n_{trees} and m_{try}. They found the optimal number of trees to be $n_{trees} = 1000$ and the m_{try} is 4.

Another study Hussain et al. (2025) uses a Random Forest approach to examine drought as measured by the SPI-03. The geographic area is in Punjab, Pakistan. They test their results by comparing it to a logistic regression. The data used is monthly data from 1981 to 2021, with 70% for training and 30% for validation. It is not explicit what the hyperparameter selection is.

Dikshit et al. (2020) also applies Random Forest models to analyse droughts in New South Wales (NSW), Australia. They computed SPEI using data from the Climatic Research Unit (University of East Anglia). They train using data from 1901 to 2010, validate the model from 2011 to 2015, and test the model on the period from 2016 to 2018. The explanatory variables are rainfall, potential evapotranspiration (PET), vapour pressure, cloud cover, and temperature. As expected, the most important variables are rainfall and temperature. They train the model using random search and grid search methods for hyperparameter selection. The study follows objectives similar to this Essay, as it produces a gridded forecast.

Artificial Neural Networks (ANNs) are based on a mathematical model of the brain and are then applied to nonlinear regression analysis Ripley (1994). An ANN consists of interconnected neurons arranged in layers. The input layer receives the predictor variables. In a simple neural network without a hidden layer, the input layer is a linear combination of the

output layer (similar to regression). The hidden layer contains the neurons where the core data processing occurs. In forecasting applications, an ANN learns complex, nonlinear relationships between a dependent variable and its predictors. Inside those neurons, the inputs are transformed using linear and non-linear combinations. The output layer will be where the prediction is. The network will try to minimise a loss function by properly selecting the prediction of the dependent variable.

Following Kuhn and Johnson (2013), each neuron k in the hidden layer first computes a linear combination of the predictor variables x_j using a set of weights β_{jk} and a bias term β_{0k}. This linear combination is then transformed by a nonlinear activation function $g(\cdot)$. Formally,

$$u = \beta_{0k} + \sum_j x_j \beta_{jk}, \tag{5}$$

and the output of neuron k is defined as

$$h_k(x) = g(u), \tag{6}$$

where $g(\cdot)$ is commonly chosen as a sigmoid activation function:

$$g(u) = \frac{1}{1 + e^{-u}}. \tag{7}$$

Finally, the outputs of the hidden neurons are combined through a linear function to produce the network's prediction. Each hidden neuron contributes to the final output with an associated weight γ_k:

$$f(\mathbf{x}) = \gamma_0 + \sum_{k=1}^{H} \gamma_k h_k. \tag{8}$$

The hyperparameters that need to be chosen by the researcher are now *size* and *decay*. *size* is the number of neurons in the hidden layer, and *decay* is a parameter that regulates

the weights in the network when predicting a value, penalizing larger weights.

In the drought forecasting literature, Morid et al. (2007) uses an Artificial Neural Network (ANN) to forecast SPI in the Tehran Region, Iran. They trained different models with different inputs to select the best architecture for their Neural Network, tested various networks and learning algorithms, and found feed-forward training to be the most suitable. A variety of inputs were used, including SPI lags and rainfall lags. Additionally, some models include large-scale climate indices such as the Southern Oscillation Index (SOI) and the North Atlantic Oscillation (NAO). The selected model was the one trained using SPI lags of 1 to 4 periods, a seasonal lag of 12 periods and Rainfall lags of 1 to 2. The SOI and NAO models did not perform well. This study contributes to the idea of generating an ANN only with lagged variables.

A recent study applies not only one but several machine learning methods to forecast drought. In Oyounalsoud et al. (2024), they forecast SPEI among other indicators for Alice Springs, Australia. The data is for 36 years. They use Random Forest (RF), Artificial Neural Network (ANN), and other methods (Decision Tree (DT), Generalised Linear Model (GLM), Support Vector Machine (SVM), and Deep Learning (DL)). These studies, doing ensembles of models, are quite popular in the machine learning literature. Other authors, such as Yaseen et al. (2021) and Gupta et al. (2024), also analyse a wide range of methodologies, but focus on forecasting precipitation and, with those forecasts, calculate an SPI. An interesting question arising from this paper is whether the forecast variable should be precipitation rather than the Drought Index. The question is whether the models will be able to better recognise relationships in rainfall data rather than in index data. Also, it supports the idea of generating 4 different forecasts, which I follow in this study.

2.1.3 Hybrid Model: Wavelet Transformation + ARIMA

A common approach to forecasting time series in the climate and drought literature is the Wavelet Transformation. This process decomposes the original data into multiple frequency components and then applies time-series forecasting methods to each decomposed series. The forecast of the original series is reconstructed by summing together the forecasts of the individual components.

The Wavelet Transformation was first formalised by Mallat (1989), who developed a theoretical framework for decomposing signals—initially images—into different pieces of information to obtain a new representation known as the wavelet representation. Although Mallat's goal was not time-series forecasting, subsequent developments extended wavelet theory into economics, hydrology, and climate time-series analysis.

One of the first applications in economics was performed by Ramsey and Zhang (1997), which analysed foreign exchange rates. The motivation for applying wavelet methods in forecasting is that disaggregating the original data into different frequency bands may improve predictive accuracy. Each frequency component may capture distinct patterns—short-term fluctuations or long-term trends—that traditional models may not fully exploit it when applied to the raw series. After forecasting each component separately, the final forecast is obtained by recomposing (summing) the individual forecasts.

One paper applying wavelet transformation to drought forecasting is Rezaiy and Shabri (2023). The original SPI series is first decomposed into 4 sub-series using the Discrete Wavelet Transform (DWT). The 4 series are forecasted using ARIMA models, and then the original series is reconstructed by summing the 4 forecasts. They apply the methodology to SPI at 3, 6, 9, and 12 months. Another technical detail is that, for the wavelet transformation, they use the Daubechies2 filter. The authors compare it to ARIMA and find improvements in RMSE and MAE on all SPI time scales.

Other studies apply the wavelet transformation method and use multiple forecasting methodologies depending on the forecasted frequency. Khan et al. (2020) employs this technique on the SPI. Using 30 years of monthly rainfall data (1986 to 2016) from the Langat River Basin, Malaysia. The wavelet transformation produces low-frequency series, which are modelled using ARIMA, while the high-frequency series is modelled using ANN methods. They argue that high-frequency signals are not linear and that ANNs perform better with this type of structure. For the low-frequency, they follow the reviewed ARIMA methodology, identifying the best model using Information Criteria. Another similar approach was followed by Wu et al. (2021), but with rainfall forecasting rather than the drought index. Their methodology is to disaggregate the original series, then forecast the low-frequency using ARIMA, and solve the high-frequency problem using a Long Short-Term Memory (LSTM) model.

One parameter in the wavelet transformation process is the filter used. There are several methods, and Polanco-Martínez, Fernández-Macho, and Medina-Elizalde (2020) says that the Daubechies Least Asymetric 8 (LA(8)) works better for Climate Series.

2.1.4 Other determinants of Droughts

Notable works focused on climatological and physical models are valuable for modelling droughts. Studies such as Chiang, Mazdiyasni, and AghaKouchak (2021), Gebrechorkos et al. (2025), and S. Wang, Hipps, Gillies, and Yoon (2014) may be useful for integrating explanatory variables into future research for forecasting purposes.

One potential explanatory variable is anthropogenic emissions, which contribute to climate change (by affecting temperature and, in turn, drought). Chiang et al. (2021) used different precipitation values from the model CMIP6. They compared historical data with the natural-only model simulation (which excludes anthropogenic aerosol emissions). Using this data, the authors recreate an SPI Drought Index (only with precipitation data) and find

that anthropogenic aerosols have influenced droughts in different regions of the world. By expanding their analysis to include Potential Evapotranspiration, they find an even greater likelihood of drought.

In Gebrechorkos et al. (2025), the focus is on what factors contribute to droughts. Instead of PET, they use a concept called atmospheric evaporative demand (AED), which is a broader definition of PET. Ensembling different global drought datasets and data from 1901-2022, they find that AED has increased in importance for drought severity by an average of 40%. They use and combine datasets to recreate a SPEI Index collecting data from MSWEP ((Beck et al., 2019))and CHIRPS (Climate Hazards Center (2025)) for precipitation and GLEAM (Miralles et al. (2025) and hPET(Singer et al. (2021) for AED, creating 4 different indexes. These findings support the importance of using SPEI, including PET.

Another major part of the climate literature and the relationship with Droughts is to follow the impact of the different climate patterns. S. Wang et al. (2014) studied climate patterns in the Pacific Ocean, specifically: ENSO (El Niño Southern Oscillation) and the Pacific decadal oscillation - a pattern of climate variability and a main driver of the North Pacific climate. They focus on the 2013-2014 drought in California. Using the Community Earth System Model (CESM), they analysed a ridge (a relatively high atmospheric pressure region) that formed in the western North Pacific, deepening a trough (a relatively low atmospheric pressure region) in the northeastern U.S. region. They traced this anomaly to the precursors to El Niño-Southern Oscillation (ENSO), attributable to the greenhouse gas footprint. Others, like Klavans et al. (2025), compared several climate model simulations and focused on the Pacific Decadal Oscillation (PDO). Potentially being one of the determinants of droughts in British Columbia and the western United States. Using attribution techniques, they conclude the PDO trend can be attributed to anthropogenic emissions.

If regressors were required for drought forecasting, the data availability is not a majro problem. Variables such as temperature and precipitation are available in a variety of

databases (for the context of this Essay, I analysed Beaudoing, Rodell, and NASA/GSFC/HSL (2020)). Others, like ENSO and PDO, are also found in indices. The problem arises when calculating an out-of-sample forecast. In the methodologies proposed in this Essay, any potential regressor included will require a forecast to predict the drought index.

2.2 Forecasting Performance

Once a model is trained, it may have a good fit to the historical observations used as training data, but there is no certainty about the performance when predicting future values, which is the goal of the forecasting process. An out-of-sample forecast evaluation is required to assess the model's forecasting performance.

The tools used in this Essay to test for Forecasting Performance are the Root Mean Squared Errors (RMSE), Mean Absolute Errors (MAE), and Diebold-Mariano Test (Diebold & Mariano, 1995).

2.2.1 Root Mean Squared Error and Mean Absolute Error

The Root Mean Squared Errors calculation starts with the calculation of the error term, defined as the forecasted value $\hat{y}_t$ minus the observed value y_t. The result is then squared to prevent negative values and then averaged, dividing by T, the total number of forecasted periods. This is called the Mean Squared Error. The last step for the calculation is to calculate the square root of the Mean Squared Error.

$$\text{MSE} = \frac{1}{T}\sum_{t=1}^{N}(\hat{y}_t - y_t)^2 \tag{9}$$

$$\text{RMSE} = \sqrt{\frac{1}{T}\sum_{t=1}^{T}(\hat{y}_t - y_t)^2}. \tag{10}$$

A disadvantage of the RMSE is that it penalizes larger errors more than smaller ones. A second option is the Mean Absolute Error (MAE). This index handles negative values using

the Absolute Term.

$$\text{MAE} = \frac{1}{T}\sum_{t=1}^{T}|\hat{y}_t - y_t| \tag{11}$$

The lower the RMSE or MAE, the better the model. However, we require a formal test to compare different forecasts using RMSE and MAE and conclude that we have a statistically significantly lower RMSE or MAE.

2.2.2 Diebold Mariano Test

The Diebold Mariano Test (Diebold & Mariano, 1995) is a formal test to compare the performance between a pair of forecasts. The test start with the definition of a loss function $g(\epsilon_{1t})$ and $g(\epsilon_{2t})$. The forecast errors are calculated for both forecasts as $\epsilon_1 = \hat{y}_{1t} - y_t$ and $\epsilon_2 = \hat{y}_t - y_t$. One possible definition for the loss function is the squared error loss, $g(\epsilon_{1t}) = \epsilon_{1t}^2$:

$$\bar{d} = \frac{1}{T}\sum_{t=1}^{T}(\epsilon_{1t}^2 - \epsilon_{2t}^2). \tag{12}$$

The main assumption is that if both forecasts have the same accuracy, $E(\bar{d}) = 0$; hence, a Null Hypothesis for this test is $H_0 : \bar{d} = 0$. Under the null, it can be standardized as follows:

$$DM = \frac{\bar{d}}{\hat{Var}(\bar{d})} \xrightarrow{d} N(0,1), \tag{13}$$

One extension of the Diebold Mariano test was done by Harvey, Leybourne, and Newbold (1997). They were concerned about the performance of the original test with small samples, which is often the case with forecast methods (this study aims to forecast for up to 24 months). The argument was that, for small samples, the statistic's variance should be corrected, which changes both its calculation and its distribution. The approach is to introduce a correction to the original DM indicator, based on the total number of forecast observations generated, T, and the forecast horizon h being evaluated. The corrected statistic will be now $DM*$, defined as:

$$DM^* = DM[\frac{T+1-2h+\frac{h(h-1)}{T}}{T}]^{\frac{1}{2}} \xrightarrow{d} t_{T-1}, \tag{14}$$

The "forecast" package in R (R. J. Hyndman and Khandakar (2008)) includes the function dm.test to perform a Diebold-Mariano test, and it presents the DM Statistic and p-value using the methodology of Harvey et al. (1997). This is the methodology followed in this Essay.

3 Available Data

SPEI stands for Standardised Precipitation-Evapotranspiration Index, a multi-scalar drought index that allows comparison of drought severity over time and space (Vicente Serrano et al., 2010). The authors also publish a database containing the calculations for the index. The SPEI Global Database (Beguería, Vicente Serrano, Reig-Gracia, & Latorre Garcia, 2023) is a global database with a resolution of 0.5 x 0.5 degrees. The data is available monthly from 1901 to 2022. The Index is calculated at different time scales: SPEI 1 month, SPEI 12 months, SPEI 24 months, SPEI 36 months, and SPEI 48 months.

In this Essay, SPEI-12 months is used. SPEI-12 reflects the difference between precipitation and potential evapotranspiration over 12 months and is a proper indicator of persistent Droughts.

As the SPEI is a global gridded dataset, it is possible to produce data from any geography; in this study, I focus only on North America (Canada, the United States, and Mexico). In total, there are 11,871 pixels ordered on a World Geodetic System WGS 84, the global standard geodetic reference system (latitude and longitude).

Figure 1 shows different time scales of SPEI for Victoria BC (lon -123.75, lat 48.75). It can be observed that SPEI-01 is more volatile, responding more quickly to rainy months or hot months. SPEI-06 and SPEI-12 move slowly, reacting more slowly to a rainy month or a dry month.

Figure 1: SPEI Index at different time scales for Victoria, BC

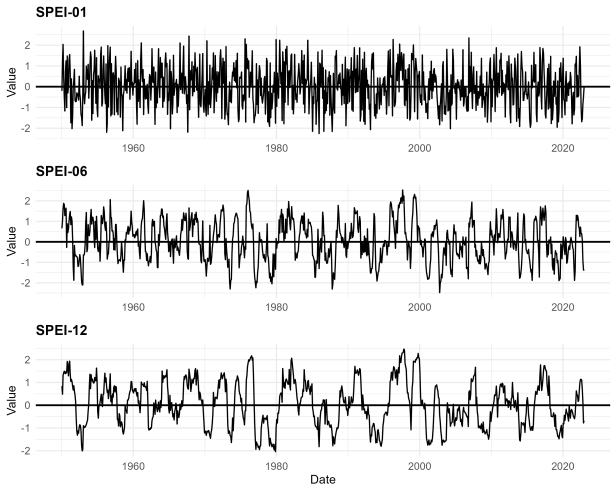

In Figure 2, the values for June 2020 and December 2020, June 2022 and December 2022 are presented. The figure shows the spatial and temporal patterns of drought. In June 2020, the West of the United States was experiencing a mild drought; within 6 months, it was now a severe drought and expanded north. In Canada, in June 2020, only Quebec and the Atlantic were experiencing milder droughts; two years later, the situation was worse in the Northwest Territories and Nunavut, which have a polar climate. Vancouver Island and the west coast were also experiencing moderate droughts. Drought is spatially dependent and can occur across a wide range of climates.

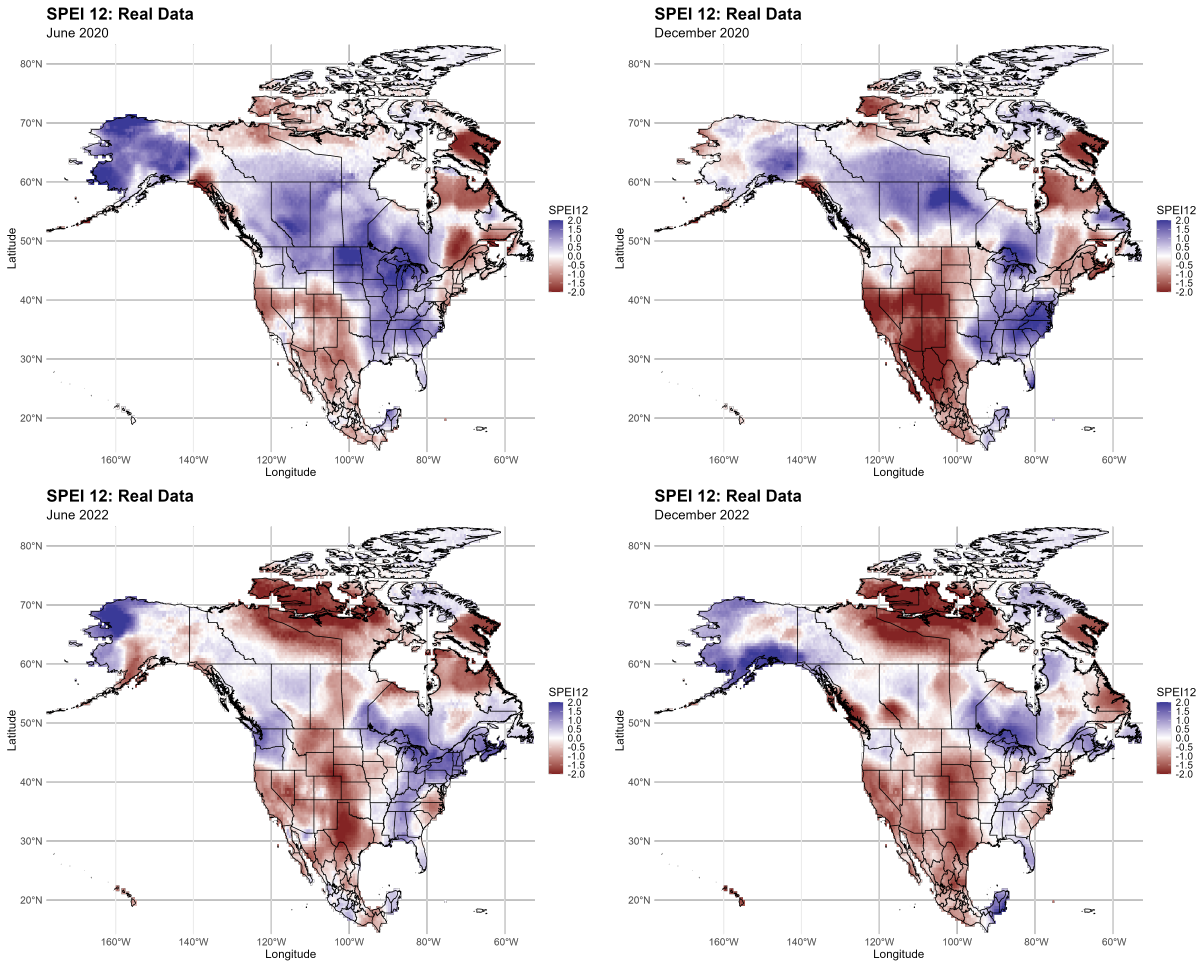

Figure 2: Spatial Distribution of Drought 2020-2022

4 Methodology

I trained four models to forecast the drought index SPEI-12 using the SPEI V2.0 database (Beguería et al. (2024)). I used different forecasting models: Seasonal ARIMA, Random Forests (750 trees, hyperparameters tuned over a grid $m_{try} \in \{2, 4, 6, 8, 10\}$ and $min.node.size \in \{5, 10, 20\}$), Artificial Neural Networks (single hidden layer; tuning grid: $size \in \{3, 7, 11\}$, $decay \in \{0.001, 0.01, 0.1\}$), and Wavelet Transformation+ARIMA. I exploit the gridded structure of the SPEI Global database to generate one trained model for each pixel and a methodology for the North American continent (Canada, the United States, and Mexico).

The four models trained are meant to be autoregressive, only training on lags of the same SPEI-12 and a moving-average term in the ARIMA and Wavelet models. This aligns with most cases in the literature. Few papers in the literature include additional regressors, such as rainfall, temperature, or evapotranspiration data. Others suggest including some climate phenomena, such as the El Niño–Southern Oscillation (ENSO), as a next step. The problem with including any of these variables is the need for properly forecasted data to create a real out-of-sample forecast. That is why, for this Essay, I decided to focus on the autoregressive characteristics.

4.1 S-ARIMA model

For the training of the Seasonal ARIMA models: $AIRMA(p, d, q)(P, D, Q)[12]$ models, a monthly frequency is maintained. The data is divided into a training set and a test set, with the last 24 months reserved for the test set. The first step is to test the series for stationarity. As the SPEI is always centered at 0, it is expected to be stationary. As a second step, I run an ACF and a PACF to understand the presence of seasonality. Figure 3 shows it. The next step follows an iterative process of training and testing different model specifications. Each pixel is tested at different levels of p, d, q, and P, D, Q, and the Information Criteria is calculated for each one.

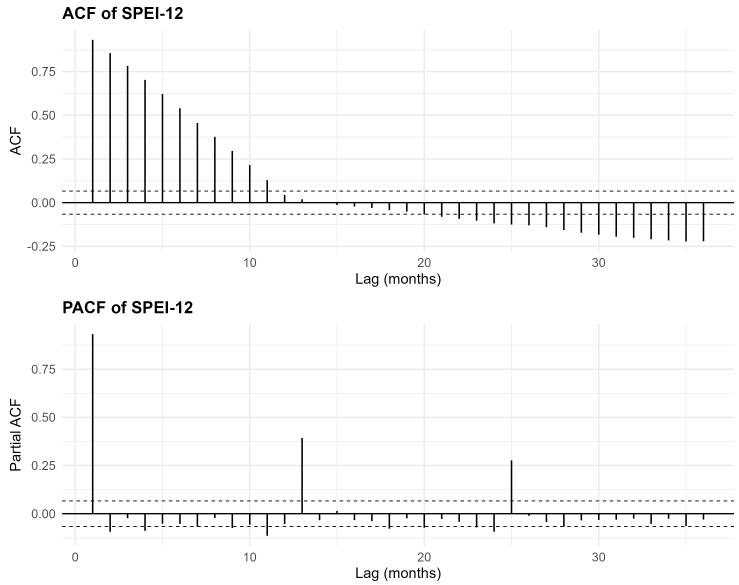

Figure 3: ACF and PACF of the SPEI-12 series for the Victoria pixel

The ARIMA model is selected using Information Criteria, where the model with the minimum AIC is chosen. The selection process evaluates models on the complete set of parameters $AIRMA(p,d,q)(P,D,Q)[12]$. Only for British Columbia, I train models using the BIC Information Criteria. I tested it, and there are no differences in the accuracy.

I also completed a residual evaluation. Tests for residual autocorrelation, conditional heteroskedasticity, and residual normality were performed. As the objective is to forecast, these requirements are less strict; nevertheless, the test can provide more diagnostic information about the models if needed.

The last step in the methodology for Seasonal ARIMA models is to forecast 24 months (H = 24) and then test its accuracy on a test set. This forecast is dynamic: the first month is forecast using the model, and that forecast is used, if required, as a lag in the second-month prediction. Performance is evaluated by calculating RMSE and MAE.

The process is run in R using the packages "forecast" by R. J. Hyndman and Khandakar (2008) and R. Hyndman et al. (2025). Functions used are "auto.arima", "forecast", and

"accuracy".

4.2 Random Forest model

For the Random Forest Model, a similar approach is used for the training and test sets. Unlike ARIMA models, where the lags are determined within the process using Information Criteria, the Random Forest Model requires predetermined lags to be set in advance to learn from them.

The first step in the Random Forest methodology is to construct these lags. The ACF and the PACF suggested a strong short-term correlation and seasonal dependence at the seasonal lags 12 and 24. (see Figure 3). Based on this, the lags introduced in the trained models were from 1 through 6, as well as seasonal lags at 12 and 24 months. It includes a dummy indicating the month and a trend value.

By design, random forests randomly sample observations. For time series, this will imply that the time characteristic would be broken. To avoid this problem, and following the literature, I used a cross-validation time-lapse approach, following Kuhn (2007). This will generate samples using a random initial date, with a 120-period (10-year) training set and 2 years more for validation. The validation set will be used to test the performance of the hyperparameters. Doing this, the temporal order will be respected.

The number of trees selected for the training is 750. In the literature, the number of trees ranges from 500 to 1,000. Increasing the number of trees generally improves the results but also increases computational cost. After experiments with a small number of pixels, I decided to balance predictive performance and computation time across 750 trees.

The hyperparameters were tuned using a grid-search strategy, which ensures the evaluation of all possible combinations of $m_{try} \in \{2, 4, 6, 8, 10\}$ and $min.node.size \in \{5, 10, 20\}$). The grid search evaluates each candidate configuration and selects the best combination of m_{try} and $min.node.size \in \{5, 10, 20\}$ that yields the best forecast performance (lowest

cross-validated RMSE).

Using Random Forest, a measure of the importance of the input variable can be presented. Variable importance measures how much each predictor contributes to improving prediction accuracy or reducing error across the entire model. This is computed for each model in each pixel.

After the training, a dynamic forecast is performed by feeding the model the first period of data from the test set, $h = 1$, and predicting the value. The predicted values are used as lags to calculate the next period until $h = 24$ is reached. Performance measures, RMSE and MAE, are calculated and stored.

The Random Forest process is run in R using the packages "caret" by Kuhn (2008) and "ranger" by Wright and Ziegler (2017).

4.3 Artificial Neural Network model

The Artificial Neural Network is calibrated as follows: single hidden layer; tuning grid: $size \in \{3, 7, 11\}$, $decay \in \{0.001, 0.01, 0.1\}$.

As with the Random Forest model, the lags in the training data need to be selected before training. The same lag structure selected for Random Forest was used in ANN: 1-6 months of lag data, and seasonal lags of 12 and 24 months. Similarly, I used a cross-validation time-lapse approach with 120 periods for the training set and 24 periods for the validation set. A grid search strategy was used for the Artificial Neural Network. The hyperparameters to be chosen are,: $size \in \{3, 7, 11\}$ and $decay = 0.001, 0.01, 0.1$. This will evaluate all possible hyperparameter combinations.

After the training, the dynamic forecast is generated using the same process as Random Forest. The performance measures, RMSE and MAE, are calculated and stored.

The Artificial Neural Network process is run in R using the packages "caret" by Kuhn (2008) and "nnet" by Venables and Ripley (2002).

4.4 Wavelet Transformation

The first step in the wavelet transformation process is the disaggregation of data into different frequencies.

I decided to disaggregate the data into 4 different waves, following the literature. The method used for the disaggregation was the Maximum Overlap Discrete Wavelet Transform, mainly because it maintains the time periods. The methodology also requires a filter; there are several, but I chose LA(8) (least asymmetric) according to the literature on climate time series. The 4 shows the 4 different waves, and the original data for Victoria, B.C., is presented. The sum of the 4 different waves is the original value.

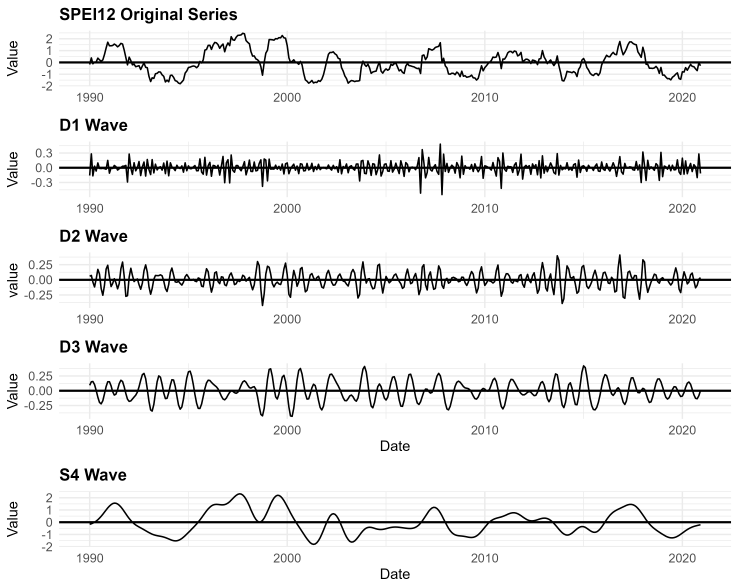

Figure 4: Wavelet Transformation for Victoria, BC

The next step is to proceed with the training models. The methodology here is similar to that used for the ARIMA models. We will have 4 different trained models.

After the training, 4 forecasts are calculated, and then summarized to return the forecast for the original data.

The Wavelet Transformation process is run in R using the package "wavelets" by ? (?),

using the function "mra". ARIMA models are trained using the "forecast" package by R. J. Hyndman and Khandakar (2008) and R. Hyndman et al. (2025) and the "auto.arima" function.

4.5 Training Set and Test Set

I split the data into two sections: the training set and the test set (not to be confused with the validation period in Random Forest and ANN methods, which is used for hyperparameter tuning). Initially, I used train data from 1950 to 2020 (70 years), and the test set from 2020 to 2022 (24 months). One challenge identified in the first attempts to train models was the high computational power required. The SPEI Global database on North America provides information on 11,871 pixels. I conducted some experiments and tested the procedure on selected pixels, focusing on different cities across North America with varying climates and locations.

In Tables 2, 3, 4, and 5, I show the results of RMSE on different starting times for the training set. The first column, 1950, is the model with 70 years of data. The last column, 2000, is the model using only 20 years. The bolded number highlights the minimum RMSE. For the ARIMA methodology, 1950 was the model with the minimum RMSE for 3 cities, and 1990 for two. Similar results were obtained with Random Forest, ANN, and Wavelet Transformation.

Table 2: ARIMA Model (AIC): RMSE (12 months) by dataset (Row Minimum in Bold)

id	Pixel ID	1950	1960	1970	1980	1990	2000
1	Victoria, BC	0.296	0.297	**0.288**	0.297	0.292	0.300
2	Vancouver, BC	**0.250**	0.259	0.251	0.255	0.250	0.254
3	Dallas, TX	**0.256**	0.422	0.479	0.361	0.272	0.815
4	Houston, TX	**0.289**	0.389	0.392	0.374	0.397	0.397
5	San Francisco, CA	1.180	1.157	1.155	**0.898**	1.090	0.932
6	Los Angeles, CA	0.723	0.705	0.716	0.705	**0.583**	0.636
7	Monterrey, MX	0.746	0.752	0.805	0.813	**0.694**	0.833

Table 3: Random Forest: RMSE (12 months) by dataset (Row Minimum in Bold)

id	Pixel ID	1950	1960	1970	1980	1990	2000
1	Victoria, BC	**0.400**	0.456	0.465	0.460	0.437	0.416
2	Vancouver, BC	0.535	0.389	0.362	**0.346**	0.435	0.403
3	Dallas, TX	0.417	0.426	0.419	0.409	0.407	**0.352**
4	Houston, TX	0.538	0.532	0.527	0.517	**0.491**	0.521
5	San Francisco, CA	0.464	**0.371**	0.448	0.947	0.633	0.781
6	Los Angeles, CA	**0.333**	0.353	0.396	0.475	0.555	0.460
7	Monterrey, MX	**0.698**	0.899	0.936	0.928	0.930	0.926

Table 4: ANN: RMSE (12 months) by dataset (Row Minimum in Bold)

id	Pixel ID	1950	1960	1970	1980	1990	2000
1	Victoria, BC	0.603	0.507	0.685	0.886	0.577	**0.440**
2	Vancouver, BC	0.406	**0.301**	0.382	0.401	0.377	0.341
3	Dallas, TX	0.399	**0.327**	0.348	0.384	0.591	0.637
4	Houston, TX	0.472	0.410	0.367	**0.318**	0.580	0.645
5	San Francisco, CA	0.912	0.762	**0.713**	0.985	2.109	1.977
6	Los Angeles, CA	0.708	**0.444**	1.056	0.462	0.794	0.617
7	Monterrey, MX	0.586	**0.478**	1.147	0.764	0.596	1.167

Table 5: Wavelet Transformation + ARIMA: RMSE (12 months) by dataset (Row Minimum in Bold)

id	Pixel ID	1950	1960	1970	1980	1990	2000
1	Victoria, BC	0.578	0.437	**0.407**	0.424	0.511	0.516
2	Vancouver, BC	0.592	0.523	0.401	0.588	**0.360**	0.421
3	Dallas, TX	0.720	0.495	0.759	**0.252**	0.326	0.509
4	Houston, TX	**0.498**	0.769	0.913	0.874	0.767	0.727
5	San Francisco, CA	2.017	1.728	2.134	1.916	**1.382**	1.561
6	Los Angeles, CA	1.153	1.173	1.478	1.187	**0.608**	0.868
7	Monterrey, MX	0.823	0.998	**0.799**	0.914	0.878	0.911

The next step is to perform a Diebold-Mariano Test to formally conclude if we are really losing forecasting power. In Tables 6, 7, 8, 9 a summary is presented. The Diebold-Mariano Test shows that there is no significant difference between the forecasts.

Table 6: ARIMA Model (AIC): DM Test Statistic (Best Model given RMSE vs Other)

id	City	Best Year	1950	1960	1970	1980	1990	2000
1	Victoria, BC	1970	-0.49	-0.47	NA	-0.51	-0.44	-0.26
2	Vancouver, BC	1950	NA	-0.21	0.45	-0.64	0.67	-0.54
3	Dallas, TX	1950	NA	0.60	0.52	0.67	0.23	-1.03
4	Houston, TX	1950	NA	0.56	0.55	0.60	0.55	0.55
5	San Francisco, CA	1980	-4.14	-2.05	-1.90	NA	-2.38	-0.25
6	Los Angeles, CA	1990	-1.89	-1.83	-1.68	-1.70	-1.32	NA
7	Monterrey, MX	1990	-0.41	-0.42	-0.67	-0.53	-0.90	NA

Table 7: Random Forest: DM Test Statistic (Best Model given RMSE vs Other)

id	City	Best Year	1950	1960	1970	1980	1990	2000
1	Victoria, BC	1950	-0.94	-1.15	-1.14	-1.13	-1.02	NA
2	Vancouver, BC	1980	0.23	-0.99	NA	0.06	0.39	-0.09
3	Dallas, TX	2000	-1.39	-1.35	-1.35	-1.16	NA	-1.44
4	Houston, TX	1990	-1.13	-2.01	-2.06	NA	0.05	-1.23
5	San Francisco, CA	1960	NA	-0.65	-0.93	-2.00	-3.79	-0.60
6	Los Angeles, CA	1950	0.64	0.43	0.34	-1.13	0.17	NA
7	Monterrey, MX	1950	-0.79	-0.83	-0.82	-0.83	-0.81	NA

Table 8: ANN: DM Test Statistic (Best Model given RMSE vs Other)

id	City	Best Year	1950	1960	1970	1980	1990	2000
1	Victoria, BC	2000	0.13	0.20	-0.03	0.42	NA	-0.89
2	Vancouver, BC	1960	0.53	-1.02	-0.49	-0.66	0.56	NA
3	Dallas, TX	1960	0.25	0.87	0.84	0.62	-1.24	NA
4	Houston, TX	1980	0.60	0.73	NA	0.61	0.58	0.75
5	San Francisco, CA	1970	-2.08	NA	0.21	-0.82	-0.69	-0.87
6	Los Angeles, CA	1960	-0.97	-1.85	-0.89	-0.24	-0.85	NA
7	Monterrey, MX	1960	-1.08	-1.11	-0.78	-0.73	-1.11	NA

Table 9: Wavelet Transformation + ARIMA (AIC): DM Test Statistic (Best Model given RMSE vs Other)

id	City	Best Year	1950	1960	1970	1980	1990	2000
1	Victoria, BC	1970	-2.02	0.32	0.41	-0.19	-1.38	NA
2	Vancouver, BC	1990	-0.46	-2.60	-0.51	NA	-0.89	-1.11
3	Dallas, TX	1980	-1.95	-1.50	NA	-0.90	-2.74	-2.61
4	Houston, TX	1950	NA	-1.27	-1.31	-1.96	-1.29	-1.49
5	San Francisco, CA	1990	-1.34	-2.42	-2.09	NA	-3.11	-1.42
6	Los Angeles, CA	1990	-4.25	-3.76	-3.74	NA	-2.16	-1.97
7	Monterrey, MX	1970	-0.05	-0.77	-0.70	-0.40	-1.84	NA

Based on these results, the decision was to set 1990 as the starting year for the training set and to use 30 years of data to train all models, which improved the computational efficiency. On a standard computer, training the four models for a single pixel took approximately 7 minutes using data from 1950 onward. Using data starting in 1990 reduced training time to about 3 minutes, a 64% reduction in computation time.

5 Results

I summarise the results of the methods for a single pixel, in this case, Victoria, BC (lon -123.75, lat 48.75). All the results for Victoria are also available for the remaining 11,870 pixels in North America. Later, I will discuss the model's performance using a map visualization. The final part of the results shows the Ensemble of models, with a visualization showing the model with the minimum RMSE for each pixel.

The Figure 5 summarizes the 4 different forecasts for the 24-month period for Victoria, BC. For the first months, S-ARIMA follows the observed values and reacts to sudden changes in direction. However, after 1 year, the model reaches the long-run mean and becomes practically flat. Another model with notable performance is the ANN Model, which follows the trend of the original series in December 2021 and also decreases as observed values decrease at the end of 2022; however, not in the expected magnitude. Random Forest and

Wavelet+ARIMA models don't appear to follow the series in the first year; however, Random Forest reaches the observed value in the second year, in December 2022. None of the models captured a sharp increase in the SPEI value in June 2022. Other regions may follow different dynamics.

Figure 5: Forecast by methodology and Error Comparative of Victoria BC

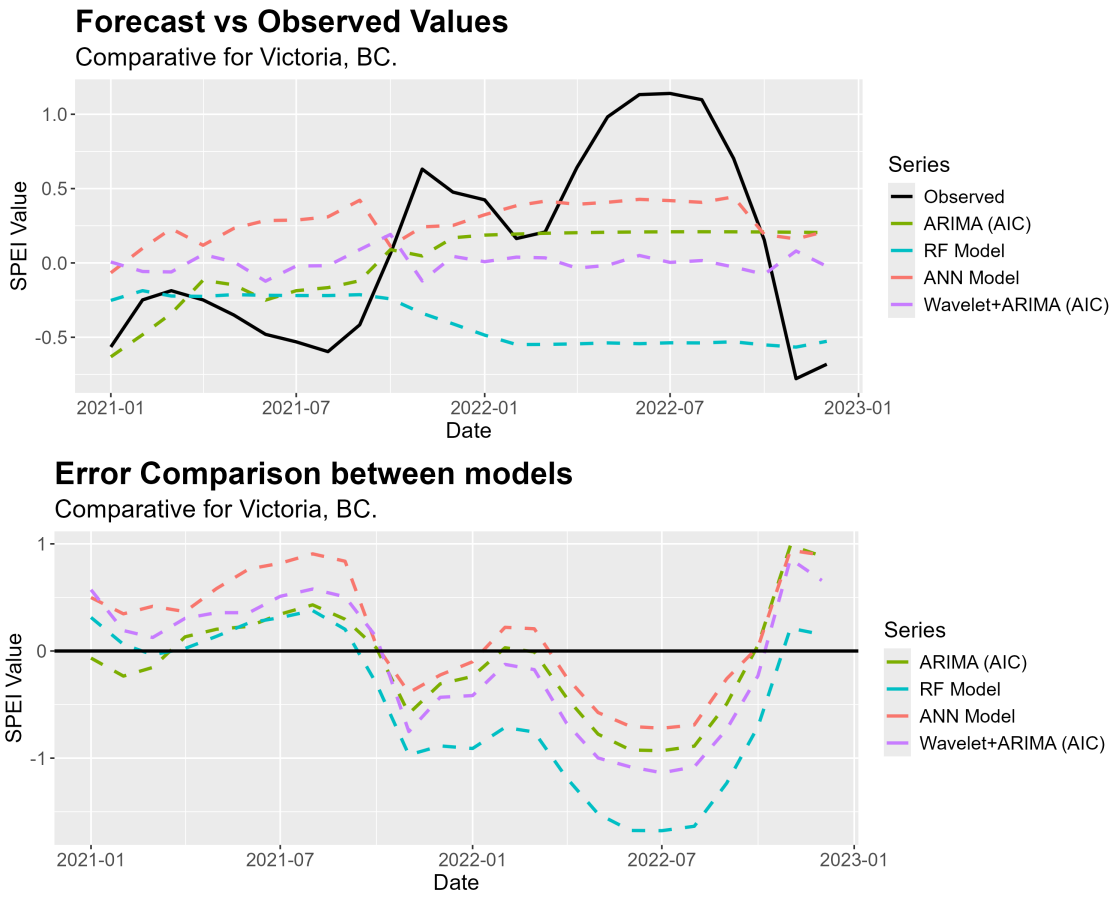

In Table 10, I present the results for ARIMA models. For British Columbia (Victoria, B.C included), I produced two models with two different Information Criteria: AIC and BIC. For AIC, the selected model was ARIMA(3,0,1)(0,0,1)[12], while the BIC was ARIMA(3,0,0)(0,0,1)[12]. In Figure 3, the ACF and the PACF are presented. The ACF suggests that Victoria has AR characteristic. The PACF suggests it may be AR(1); it also shows the seasonal component. An interesting result is that the ARIMA function didn't

capture the seasonal component.

Table 10: Results for Victoria BC: ARIMA Best Model using AIC

	AIC Model	BIC Model
AR(1)	1.995^{***}	1.109^{***}
	(0.072)	(0.052)
AR(2)	-1.079^{***}	-0.100
	(0.119)	(0.078)
AR(3)	0.081	-0.031
	(0.053)	(0.052)
MA(1)	-0.914^{***}	
	(0.051)	
S-MA(1)	-0.784^{***}	-0.783^{***}
	(0.039)	(0.039)
AIC	115.910	115.838
AICc	116.140	116.001
BIC	139.423	135.432
Log Likelihood	-51.955	-52.919
Num. obs.	372	372

$^{***}p < 0.001$; $^{**}p < 0.01$; $^{*}p < 0.05$

In Table 11, I present the results for Random Forest for Victoria, BC. A total of 750 trees were created. After tuning, the hyperparameter selected in the methodology was $m_{try} = 8$ (randomly selected inputs) and a minimum node size of 20. The m_{try} and node sizes were selected via a grid search. Table 12 shows the results of the calculation of the Variable Importance. This indicator is the variable's contribution to reducing the prediction error. Lag_1 is the variable that contributes the most. The next one is Lag_2. The seasonal lags Lag_12 and Lag_24 also appear, but with marginal values.

Table 11: Random Forest model settings and cross-validated performance for Victoria, BC.

Setting	Value
Method	ranger
Number of trees	750
mtry	8
Split rule	1
Minimum node size	20
Training samples	348
CV RMSE	0.423
CV MAE	0.333
CV R-squared	0.564

Table 12: Top 10 predictors by variable importance in the RF model for Victoria, BC.

Predictor	Importance
lag_1	281.075
lag_2	48.673
lag_3	7.598
trend	5.194
lag_24	3.952
lag_12	3.723
season	2.967
lag_4	1.784
lag_5	1.631
lag_6	1.278

In Table 13, I present the results for ANN for Victoria, BC. The selected architecture is 10–3–1. Even when the grid search method enabled 7 and 11, the selected hidden units were 3. Interesting that ANN would not be able to find more nonlinear relationships.

Table 13: ANN model settings and cross-validated performance for Victoria, BC.

Setting	Value
Method	nnet
Hidden units (size)	3
Weight decay	0.1
Number of inputs	10
Training samples	348
CV RMSE	0.567
CV MAE	0.463
CV R-squared	0.45

In Figure 6, the RMSE and MAE for the ARIMA method are shown in a map of North America. Important to note that the calculations of RMSE and MAE only take into account 12 months of forecasts for the purpose of this visualization. The color pattern in this and the following maps is yellow for models with low RMSE and MAE, and purple for models with the highest RMSE and MAE. ARIMA models perform very well in the Arctic region, except on the west coast of Alaska. There is an interesting pattern in which the ARIMA model doesn't fit well, from central California to the Canadian provinces of Manitoba and Saskatchewan, extending into the Great Lakes region and finishing in Atlantic Canada. This "purple patch" in the middle of the continent encompasses a wide range of climates and geographies. Other areas where the ARIMA model struggles to perform well include the desert region of Texas, the northern part of Mexico, and southern regions in the United States, such as Mississippi and Alabama.

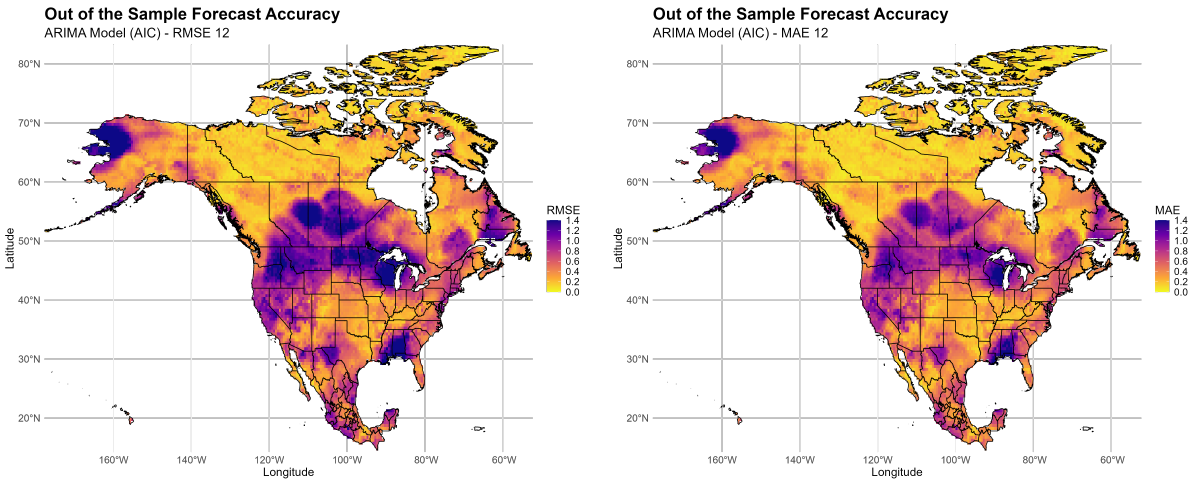

Figure 6: Forecasting Accuracy for ARIMA Model RMSE and MAE

The ARIMA model, one of the best performers, struggles to understand and forecast the drought index in different elevations, climates, latitudes, and longitudes.

In Figure 7, I show the Random Forest performance results. The regions where the model struggles are related to the ARIMA model. The Random Forest model performs better in polar regions, with lower RMSE than in other regions. For example, the Canadian Territory of Nunavut has an average RMSE of 0.235, vs. Texas at 0.794 for the Random Forest model.

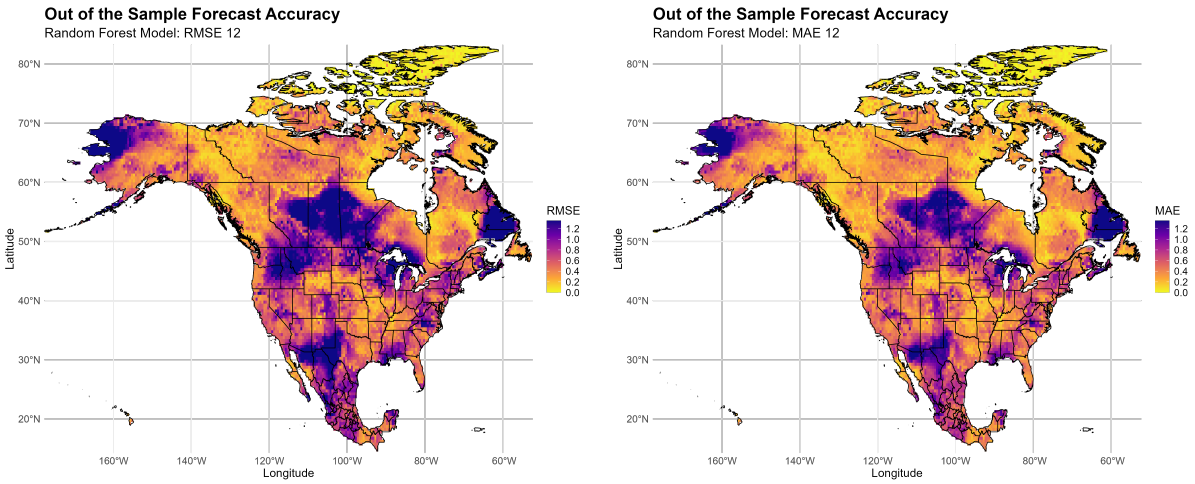

Figure 7: Forecasting Accuracy for Random Forest Model RMSE and MAE

In Figure 8, the ANN performance is shown. It also follows a pattern similar to that of

Random Forest and ARIMA. It is a bit noisier than the two previous models; while some regions are defined as yellow and have a lower RMSE, it is not surprising to find a purple pixel with a higher RMSE surrounded by yellow. Finally, in Figure 9, the map with the results of the model Wavelet+ARIMA is presented. Overall, the map shows the model has the highest RMSE and MAE among the methodologies, but it still produces decent forecasts in some areas, for example, the Yucatan Peninsula in Mexico.

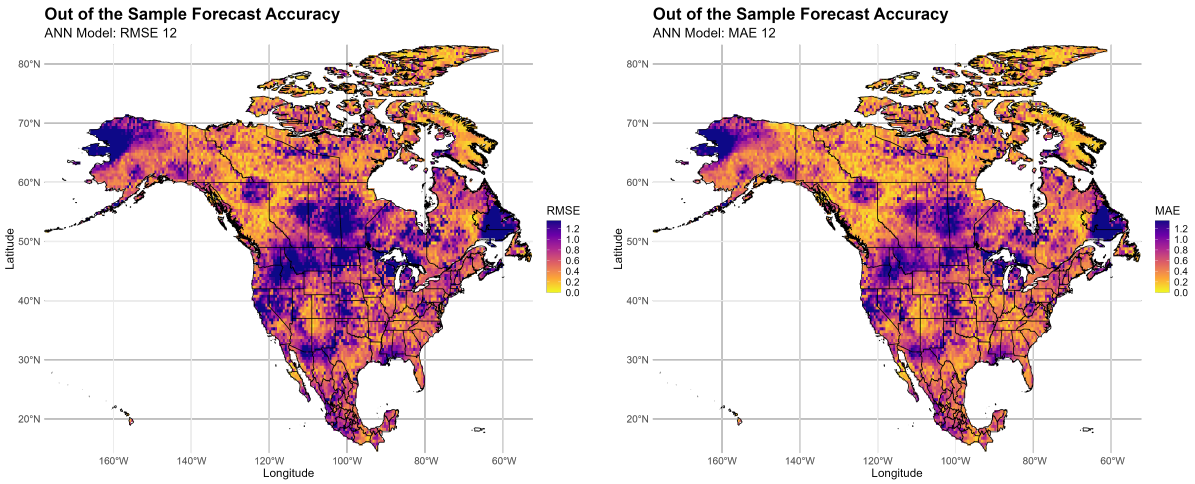

Figure 8: Forecasting Accuracy for Artificial Neural Network Model RMSE and MAE

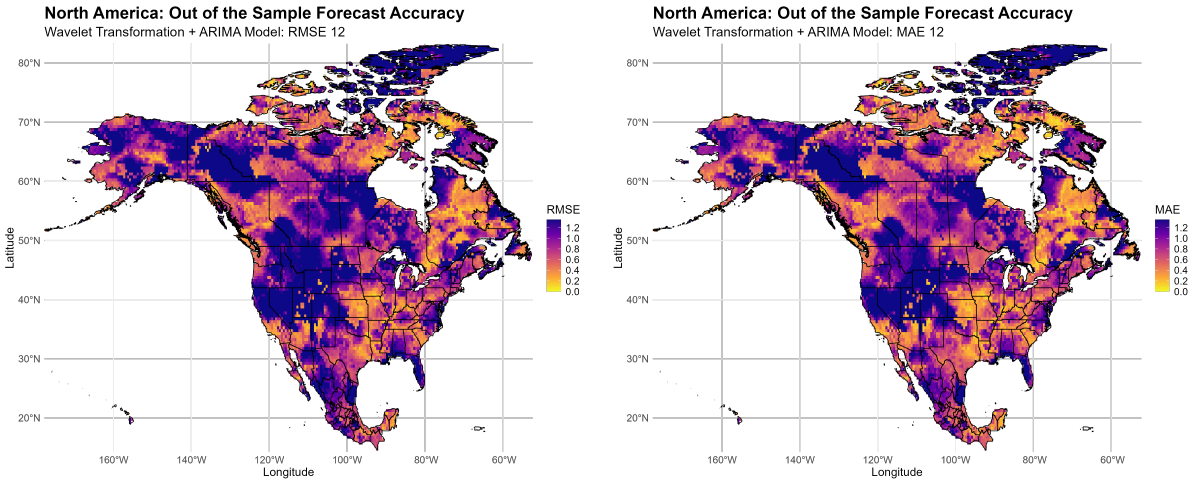

Figure 9: Forecasting Accuracy for Wavelet Transformation Model RMSE and MAE

The Ensemble forecast, which shows the combination of the lowest RMSE across the

models for each pixel, is shown in Figure 10. The map looks with fewer purple areas, as expected. However, some areas where all the models struggled can be identified. Regions like the west coast of Alaska, the Texas Desert, the north of Mexico, and the Great Lakes are where all models struggled to forecast.

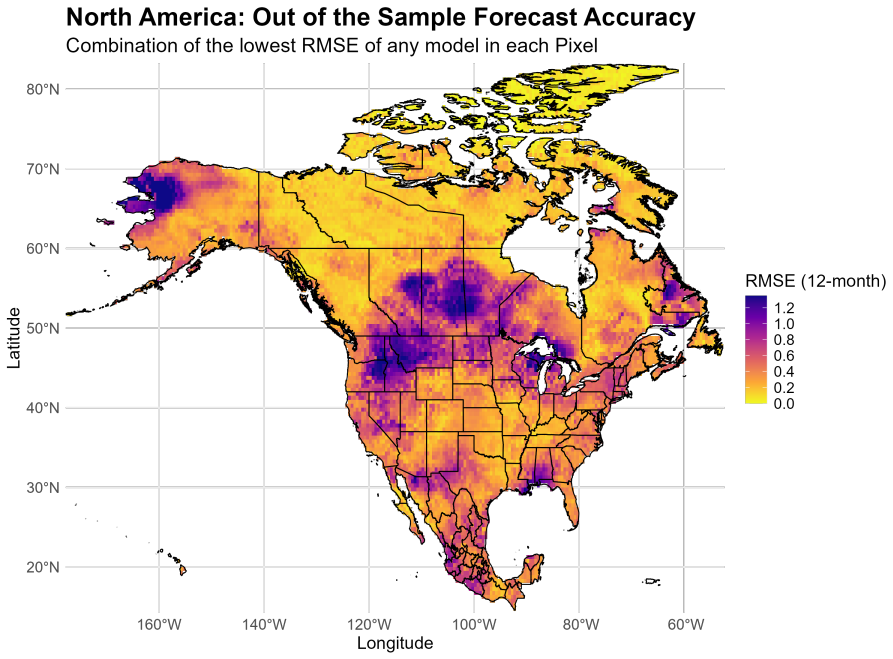

Figure 10: Combination of the lowest RMSE of any model for in each Pixel

Figure 11 presents a map summarising which model is the one with a lower RMSE. The results also follow a spatial pattern with some interesting results. Wavelet+ARIMA, overall the model with the highest RMSE, is still the model in some regions; interestingly, these regions are also the ones where other models struggled. Random Forest also performs better on the West Coast of the United States. California RMSE for Random Forest is 0.576, while for ARIMA is 0.805, ANN is 0.940, and Wavelet+ARIMA is 1.087.

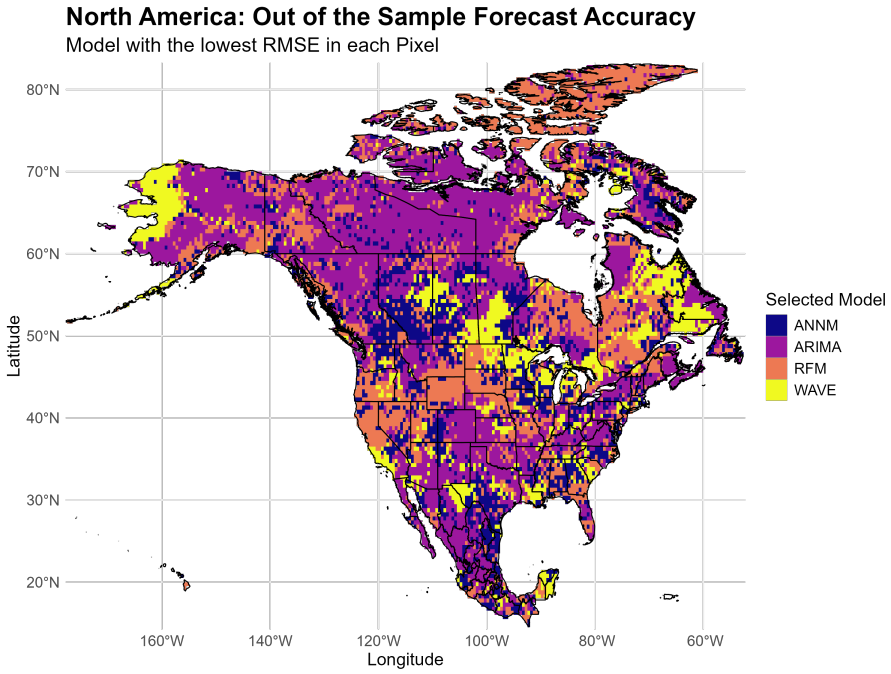

Figure 11: Model with the lowest RMSE in each Pixel

Finally, in Figure 12, I show a Diebold-Mariano Test for every pixel. The test failed to identify a significant difference in the forecast for most of the pixels. The statistically significant pixels follows a spatial pattern, with concentrations in specific regions, such as West Alaska for Wavelet Transformation+ARIMA, or North California for Random Forest.

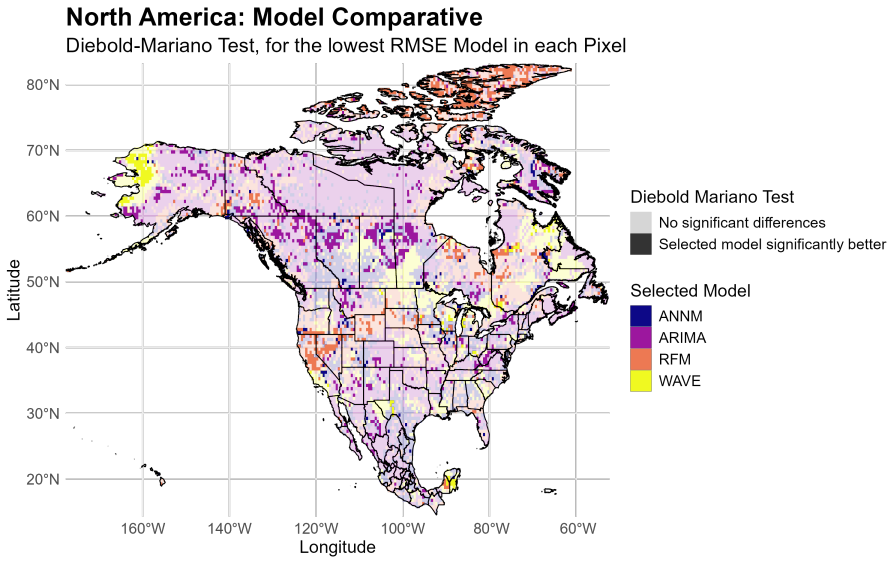

Figure 12: Diebold-Mariano Test, for the lowest RMSE Model in each Pixel

6 Next Steps and Conclusions

In this Essay, I analyzed four different forecasting methodologies and their application to the Drought Index SPEI, focused on North America (Canada, the United States, and Mexico). I presented a brief description of the drought phenomenon and how it is measured in Drought Indexes, as outlined in the climate and hydrologic literature.

The applied forecasting methods were Seasonal ARIMA, Random Forest (750 trees, hyperparameters tuned over a grid $m_{try} \in \{2, 4, 6, 8, 10\}$ and $min.node.size \in \{5, 10, 20\}$), Artificial Neural Networks (single hidden layer; tuning grid: $size \in \{3, 7, 11\}$, $size \in \{0.001, 0.01, 0.1\}$), and Hybrid models using Wavelet Transformation + ARIMA. Seasonal ARIMA is the model with the lowest overall RMSE; however, in some regions, the methodology struggles to produce reliable forecasts. Other models worked better in these areas. When formally testing forecast performance using a Diebold-Mariano Test, very few areas

actually have a statistically significant improvement in forecast performance.

The main contribution to the drought forecast literature is the type of data presented in the study. The analysis of the gridded database was not a common concept in the reviewed studies. This global, gridded database also allows this study to be recreated in other geographies.

Introducing additional regressors into the models is a potential next step for follow-up research. Variables like ENSO, Rainfall, Temperature, and altitude may have a greater role in explaining droughts, and should have forecasting power. There is more to learn from the regions where all the models failed to produce a reliable forecast. There are challenges to overcome, such as producing truly out-of-sample forecasts for each additional regressor included in the models.

This study focused on SPEI12. I chose this because I was more interested in the long-term definition of drought. Another potential next step for follow-up research may be to repeat the methodology on other time scales of the Index, such as SPEI-01, SPEI-03 (for seasonal characteristics), or SPEI-06.

Additional research questions may be asked: Is GDP growth explained by droughts? If so, a drought forecast variable may be added to the GDP growth forecast models. Additional uses of the SPEI Global database include the study of droughts and their economic consequences. Using the gridded dataset, a city-level drought index can be built, and the adaptability to droughts studied. The results and methodology discussed in this essay contribute to other research on drought and its economic consequences.

References

Achite, M., Bazrafshan, O., Azhdari, Z., Wałega, A., Krakauer, N., & Caloiero, T. (2022, March). Forecasting of SPI and SRI Using Multiplicative ARIMA under Climate Variability in a Mediterranean Region: Wadi Ouahrane Basin, Algeria. *Climate*, *10*(3), 36. Retrieved 2025-10-24, from https://www.mdpi.com/2225-1154/10/3/36 doi: 10.3390/cli10030036

Aguilar, G., & Naranjo, L. (2022). The Panama Canal: The 2015–2016 El Niño. In M. H. Glantz (Ed.), *El Niño Ready Nations and Disaster Risk Reduction* (pp. 347–360). Cham: Springer International Publishing. Retrieved 2025-12-03, from https://link.springer.com/10.1007/978-3-030-86503-0_19 (Series Title: Disaster Studies and Management) doi: 10.1007/978-3-030-86503-0_19

Akaike, H. (1974, December). A new look at the statistical model identification. *IEEE Transactions on Automatic Control*, *19*(6), 716–723. Retrieved 2025-11-29, from http://ieeexplore.ieee.org/document/1100705/ doi: 10.1109/TAC.1974.1100705

Al Sayah, M. J., Abdallah, C., Khouri, M., Nedjai, R., & Darwich, T. (2021, January). A framework for climate change assessment in Mediterranean data-sparse watersheds using remote sensing and ARIMA modeling. *Theoretical and Applied Climatology*, *143*(1-2), 639–658. Retrieved 2025-10-17, from http://link.springer.com/10.1007/s00704-020-03442-7 doi: 10.1007/s00704-020-03442-7

Azouaoui, O., & Assani, A. A. (2018, February). The case of extreme hydrologic drought downstream from reservoirs in Quebec (Canada): The intermittent flow. *River Research and Applications*, *34*(2), 135–143. Retrieved 2025-12-03, from https://onlinelibrary.wiley.com/doi/10.1002/rra.3235 doi: 10.1002/rra.3235

Beaudoing, H., Rodell, M., & NASA/GSFC/HSL. (2020). *GLDAS Noah Land Surface Model L4 monthly 0.25 x 0.25 degree, Version 2.1.* NASA Goddard Earth Sciences Data and Information Services Center. Retrieved 2025-09-21, from https://disc.gsfc.nasa.gov/datacollection/GLDAS_NOAH025_M_2.1.html doi: 10.5067/SXAVCZFAQLNO

Beck, H. E., Wood, E. F., Pan, M., Fisher, C. K., Miralles, D. G., Van Dijk, A. I. J. M., ... Adler, R. F. (2019, March). MSWEP V2 Global 3-Hourly 0.1° Precipitation: Methodology and Quantitative Assessment. *Bulletin of the American Meteorological Society*, *100*(3), 473–500. Retrieved 2025-09-21, from https://journals.ametsoc.org/view/journals/bams/100/3/bams-d-17-0138.1.xml doi: 10.1175/BAMS-D-17-0138.1

Beguería, S., Vicente Serrano, S. M., Reig-Gracia, F., & Latorre Garcia, B. (2023, July). *SPEIbase v.2.9 [Dataset].* Digital.CSIC. Retrieved 2025-12-05, from https://digital.csic.es/handle/10261/332007 doi: 10.20350/DIGITALCSIC/15470

Beguería, S., Vicente Serrano, S. M., Reig-Gracia, F., & Latorre Garcés, B. (2024, July). *SPEIbase v.2.10 [Dataset].* Digital.CSIC. Retrieved 2025-09-21, from https://digital.csic.es/handle/10261/364137 doi: 10.20350/DIGITALCSIC/16497

Box, G. E. P., Jenkins, G. M., & Reinsel, G. C. (1994). *Time Series Analysis: Forecasting and Control* (3rd ed.). Englewood Cliffs, NJ: Prentice Hall.

Breiman, L. (1996, August). Bagging predictors. *Machine Learning*, *24*(2), 123–140. Retrieved 2025-12-05, from http://link.springer.com/10.1007/BF00058655 doi: 10.1007/BF00058655

Breiman, L. (2001, October). Random Forests. *Machine Learning*, *45*(1), 5–32. Retrieved 2025-12-02, from https://link.springer.com/10.1023/A:1010933404324 doi: 10.1023/A:1010933404324

Chiang, F., Mazdiyasni, O., & AghaKouchak, A. (2021, May). Evidence of anthropogenic impacts on global drought frequency, duration, and intensity. *Nature Communications*, *12*(1), 2754. Retrieved 2025-09-19, from https://www.nature.com/articles/s41467-021-22314-w doi: 10.1038/s41467-021-22314-w

Climate Hazards Center. (2025). *CHIRPS: Rainfall Estimates from Rain Gauge and Satellite Observations.* UCSB. Retrieved 2025-12-01, from https://chc.ucsb.edu/data/chirps3 doi: 10.15780/G2JQ0P

Diebold, F. X., & Mariano, R. S. (1995, July). Comparing Predictive Accuracy. *Journal of Business & Economic Statistics*, *13*(3), 253–263. Retrieved 2025-10-16, from http://www.tandfonline.com/doi/abs/10.1080/07350015.1995.10524599 doi: 10.1080/07350015.1995.10524599

Dikshit, A., Pradhan, B., & Alamri, A. M. (2020, June). Short-Term Spatio-Temporal Drought Forecasting Using Random Forests Model at New South Wales, Australia. *Applied Sciences*, *10*(12), 4254. Retrieved 2025-12-01, from https://www.mdpi.com/2076-3417/10/12/4254 doi: 10.3390/app10124254

Dracup, J. A., Lee, K. S., & Paulson, E. G. (1980, April). On the definition of droughts. *Water Resources Research*, *16*(2), 297–302. Retrieved 2025-11-28, from https://agupubs.onlinelibrary.wiley.com/doi/10.1029/WR016i002p00297 doi: 10.1029/WR016i002p00297

Durdu, F. (2010, December). Application of linear stochastic models for drought forecasting in the Büyük Menderes river basin, western Turkey. *Stochastic Environmental Research and Risk Assessment*, *24*(8), 1145–1162. Retrieved 2025-10-17, from http://link.springer.com/10.1007/s00477-010-0366-3 doi: 10.1007/s00477-010-0366-3

Gebrechorkos, S. H., Sheffield, J., Vicente-Serrano, S. M., Funk, C., Miralles, D. G., Peng, J., ... Dadson, S. J. (2025, June). Warming accelerates global drought severity. *Nature*, *642*(8068), 628–635. Retrieved 2025-09-19, from https://www.nature.com/articles/s41586-025-09047-2 doi: 10.1038/s41586-025-09047-2

Gober, P., Sampson, D. A., Quay, R., White, D. D., & Chow, W. T. (2016, November). Urban adaptation to mega-drought: Anticipatory water modeling, policy, and planning for the urban Southwest. *Sustainable Cities and Society*, *27*, 497–504. Retrieved 2025-12-06, from https://linkinghub.elsevier.com/retrieve/pii/S2210670716300804 doi: 10.1016/j.scs.2016.05.001

Gouveia, C., Trigo, R. M., & DaCamara, C. C. (2009, February). Drought and vegetation stress monitoring in Portugal using satellite data. *Natural Hazards and Earth System Sciences*, *9*(1), 185–195. Retrieved 2025-12-06, from https://nhess.copernicus.org/articles/9/185/2009/ doi: 10.5194/nhess-9-185-2009

Gupta, B. B., Gaurav, A., Attar, R. W., Arya, V., Bansal, S., Alhomoud, A., & Chui, K. T. (2024, December). Advance drought prediction through rainfall forecasting with hybrid deep learning model. *Scientific Reports*, *14*(1), 30459. Retrieved 2025-09-23, from https://www.nature.com/articles/s41598-024-80099-6 doi: 10.1038/s41598-024-80099-6

Harvey, D., Leybourne, S., & Newbold, P. (1997, June). Testing the equality of prediction mean squared errors. *International Journal of Forecasting*, *13*(2), 281–291. Retrieved 2025-12-02, from https://linkinghub.elsevier.com/retrieve/pii/S0169207096007194 doi: 10.1016/S0169-2070(96)00719-4

Hussain, A., Niaz, R., Almazah, M. M. A., Al-Rezami, A. Y., Cheng, H., & Tariq, A. (2025, June). Utilizing Logistic Regression and Random Forest to Model Meteorological Drought Persistence Across Seasonal Transitions. *Earth Systems and Environment*. Retrieved 2025-12-01, from https://link.springer.com/10.1007/s41748-025-00682-3 doi: 10.1007/s41748-025-00682-3

Hyndman, R., Athanasopoulos, G., Bergmeir, C., Caceres, G., Chhay, L., O'Hara-Wild, M., ... Yasmeen, F. (2025). *forecast: Forecasting functions for time series and linear models*. Retrieved from https://pkg.robjhyndman.com/forecast/

Hyndman, R. J., & Khandakar, Y. (2008). Automatic Time Series Forecasting: The forecast Package for R. *Journal of Statistical Software*, *27*(3), 1–22. Retrieved from https://doi.org/10.18637/jss.v027.i03 doi: 10.18637/jss.v027.i03

IPCC. (2023). *Climate Change 2023: Synthesis Report: Contribution of Working Groups I, II and III to the Sixth Assessment Report of the Intergovernmental Panel on Climate Change*. Retrieved from https://www.ipcc.ch/report/ar6/syr/

Khan, M. M. H., Muhammad, N. S., & El-Shafie, A. (2020, November). Wavelet based hybrid ANN-ARIMA models for meteorological drought forecasting. *Journal of Hydrology*, *590*, 125380. Retrieved 2025-10-03, from https://linkinghub.elsevier.com/retrieve/pii/S0022169420308404 doi: 10.1016/j.jhydrol.2020.125380

Klavans, J. M., DiNezio, P. N., Clement, A. C., Deser, C., Shanahan, T. M., & Cane, M. A. (2025, August). Human emissions drive recent trends in North Pacific climate variations. *Nature*, *644*(8077), 684–692. Retrieved 2025-09-19, from https://www.nature.com/articles/s41586-025-09368-2 doi: 10.1038/s41586-025-09368-2

Kuhn, M. (2007, October). *caret: Classification and Regression Training.* Retrieved 2025-12-03, from https://CRAN.R-project.org/package=caret (Institution: Comprehensive R Archive Network Pages: 7.0-1) doi: 10.32614/CRAN.package.caret

Kuhn, M. (2008). Building Predictive Models in R Using the caret Package. *Journal of Statistical Software*, *28*(5), 1–26. Retrieved from https://doi.org/10.18637/jss.v028.i05 doi: 10.18637/jss.v028.i05

Kuhn, M., & Johnson, K. (2013). *Applied Predictive Modeling.* New York, NY: Springer New York. Retrieved 2025-12-05, from http://link.springer.com/10.1007/978-1-4614-6849-3 doi: 10.1007/978-1-4614-6849-3

Liaw, A., & Wiener, M. C. (2007). Classification and Regression by randomForest.. Retrieved from https://api.semanticscholar.org/CorpusID:3093707

Mallat, S. (1989, July). A theory for multiresolution signal decomposition: the wavelet representation. *IEEE Transactions on Pattern Analysis and Machine Intelligence*, *11*(7), 674–693. Retrieved 2025-11-05, from http://ieeexplore.ieee.org/document/192463/ doi: 10.1109/34.192463

McKee, T., Doesken, N., & Kleist, J. (1993). The Relationship of Drought Frequency and Duration to Time Scales. *8th Conference on Applied Climatology*, 179–184.

Miralles, D. G., Bonte, O., Koppa, A., Baez-Villanueva, O. M., Tronquo, E., Zhong, F., ... Haghdoost, S. (2025, March). GLEAM4: global land evaporation and soil moisture dataset at 0.1° resolution from 1980 to near present. *Scientific Data*, *12*(1), 416. Retrieved 2025-09-21, from https://www.nature.com/articles/s41597-025-04610-y doi: 10.1038/s41597-025-04610-y

Mishra, A. K., & Desai, V. R. (2005, November). Drought forecasting using stochastic models. *Stochastic Environmental Research and Risk Assessment*, *19*(5), 326–339. Retrieved 2025-10-17, from http://link.springer.com/10.1007/s00477-005-0238-4 doi: 10.1007/s00477-005-0238-4

Morid, S., Smakhtin, V., & Bagherzadeh, K. (2007, December). Drought forecasting using artificial neural networks and time series of drought indices. *International Journal of Climatology*, *27*(15), 2103–2111. Retrieved 2025-11-17, from https://rmets.onlinelibrary.wiley.com/doi/10.1002/joc.1498 doi: 10.1002/joc.1498

Mossad, A., & Alazba, A. (2015, March). Drought Forecasting Using Stochastic Models in a Hyper-Arid Climate. *Atmosphere*, *6*(4), 410–430. Retrieved 2025-12-01, from https://www.mdpi.com/2073-4433/6/4/410 doi: 10.3390/atmos6040410

Oyounalsoud, M. S., Yilmaz, A. G., Abdallah, M., & Abdeljaber, A. (2024, August). Drought prediction using artificial intelligence models based on climate data and soil moisture. *Scientific Reports*, *14*(1), 19700. Retrieved 2025-09-23, from https://www.nature.com/articles/s41598-024-70406-6 doi: 10.1038/s41598-024-70406-6

Palmer, W. C. (1965). Meteorological Drought. *Research Paper No. 45, U.S. Weather Bureau.* (Publisher: U.S. Government Printing Office)

Polanco-Martínez, J. M., Fernández-Macho, J., & Medina-Elizalde, M. (2020, December). Dynamic wavelet correlation analysis for multivariate climate time series. *Scientific Reports*, *10*(1), 21277. Retrieved 2025-12-02, from https://www.nature.com/articles/s41598-020-77767-8 doi: 10.1038/s41598-020-77767-8

Ramsey, J. B., & Zhang, Z. (1997, December). The analysis of foreign exchange data using waveform dictionaries. *Journal of Empirical Finance*, *4*(4), 341–372. Retrieved 2025-11-17, from https://linkinghub.elsevier.com/retrieve/pii/S0927539896000138 doi: 10.1016/S0927-5398(96)00013-8

Rezaiy, R., & Shabri, A. (2023, September). Drought forecasting using W-ARIMA model with standardized precipitation index. *Journal of Water and Climate Change*, *14*(9), 3345–3367. Retrieved 2025-10-17, from https://iwaponline.com/jwcc/article/14/9/3345/97544/Drought-forecasting-using-W-ARIMA-model-with doi: 10.2166/wcc.2023.431

Ripley, B. D. (1994). Neural Networks and Related Methods for Classification. *Journal of the Royal Statistical Society. Series B (Methodological)*, *56*(3), 409–456. Retrieved 2025-12-05, from http://www.jstor.org/stable/2346118 (Publisher: [Royal Statistical Society, Oxford University Press])

Schwarz, G. (1978, March). Estimating the Dimension of a Model. *The Annals of Statistics*, *6*(2). Retrieved

2025-11-29, from https://projecteuclid.org/journals/annals-of-statistics/volume-6/issue-2/Estimating-the-Dimension-of-a-Model/10.1214/aos/1176344136.full doi: 10.1214/aos/1176344136

Singer, M. B., Asfaw, D. T., Rosolem, R., Cuthbert, M. O., Miralles, D. G., MacLeod, D., ... Michaelides, K. (2021, August). Hourly potential evapotranspiration at 0.1° resolution for the global land surface from 1981-present. *Scientific Data*, *8*(1), 224. Retrieved 2025-09-21, from https://www.nature.com/articles/s41597-021-01003-9 doi: 10.1038/s41597-021-01003-9

Thomas, R., Davies, J., King, C., Kruse, J., Schauer, M., Bisom, N., ... Madani, K. (2024, December). *Economics of drought: Investing in nature-based solutions for drought resilience – Proaction pays* (Tech. Rep.). UN Convention to Combat Desertification (UNCCD), Economics of Land Degradation (ELD) Initiative and United Nations University Institute for Water, Environment and Health (UNU-INWEH). Retrieved 2025-12-03, from https://www.unccd.int/resources/publications/economics-drought-investing-nature-based-solutions-drought-resilience doi: 10.53328/INR24CCD001

Thornthwaite, C. W. (1948, January). An Approach toward a Rational Classification of Climate. *Geographical Review*, *38*(1), 55. Retrieved 2025-09-17, from https://www.jstor.org/stable/210739?origin=crossref doi: 10.2307/210739

Venables, W. N., & Ripley, B. D. (2002). *Modern Applied Statistics with S* (Fourth ed.). New York: Springer. Retrieved from https://www.stats.ox.ac.uk/pub/MASS4/

Vicente Serrano, S. M., Beguería, S., & López-Moreno, J. I. (2010). A Multiscalar Drought Index Sensitive to Global Warming: The Standardized Precipitation Evapotranspiration Index. *Journal of Climate*, *23*(7), 1696 – 1718. Retrieved from https://journals.ametsoc.org/view/journals/clim/23/7/2009jcli2909.1.xml (Place: Boston MA, USA Publisher: American Meteorological Society) doi: 10.1175/2009JCLI2909.1

Wang, Q., Zhao, L., Wang, M., Wu, J., Zhou, W., Zhang, Q., & Deng, M. (2022, October). A Random Forest Model for Drought: Monitoring and Validation for Grassland Drought Based on Multi-Source Remote Sensing Data. *Remote Sensing*, *14*(19), 4981. Retrieved 2025-12-01, from https://www.mdpi.com/2072-4292/14/19/4981 doi: 10.3390/rs14194981

Wang, S., Hipps, L., Gillies, R. R., & Yoon, J. (2014, May). Probable causes of the abnormal ridge accompanying the 2013–2014 California drought: ENSO precursor and anthropogenic warming footprint. *Geophysical Research Letters*, *41*(9), 3220–3226. Retrieved 2025-09-19, from https://onlinelibrary.wiley.com/doi/10.1002/2014GL059748 doi: 10.1002/2014GL059748

Wilhite, D. A., & Glantz, M. H. (1985, January). Understanding: the Drought Phenomenon: The Role of Definitions. *Water International*, *10*(3), 111–120. Retrieved 2025-09-17, from http://www.tandfonline.com/doi/abs/10.1080/02508068508686328 doi: 10.1080/02508068508686328

World Meteorological Organization, & Global Water Partnership. (2016). *Handbook of Drought Indicators and Indices* (M. Svoboda & B. A. Fuchs, Eds.) (No. 2). Geneva: Integrated Drought Management Programme (IDMP).

Wright, M. N., & Ziegler, A. (2017). ranger: A Fast Implementation of Random Forests for High Dimensional Data in C++ and R. *Journal of Statistical Software*, *77*(1), 1–17. Retrieved from https://doi.org/10.18637/jss.v077.i01 doi: 10.18637/jss.v077.i01

Wu, X., Zhou, J., Yu, H., Liu, D., Xie, K., Chen, Y., ... Xing, F. (2021, January). The Development of a Hybrid Wavelet-ARIMA-LSTM Model for Precipitation Amounts and Drought Analysis. *Atmosphere*, *12*(1), 74. Retrieved 2025-11-30, from https://www.mdpi.com/2073-4433/12/1/74 doi: 10.3390/atmos12010074

Yaseen, Z. M., Ali, M., Sharafati, A., Al-Ansari, N., & Shahid, S. (2021, February). Forecasting standardized precipitation index using data intelligence models: regional investigation of Bangladesh. *Scientific Reports*, *11*(1), 3435. Retrieved 2025-10-24, from https://www.nature.com/articles/s41598-021-82977-9 doi: 10.1038/s41598-021-82977-9

List of Figures

List of Tables